Journal of Non-Crystalline Solids 577 (2022) 121328

Contents lists available at ScienceDirect

Journal of Non-Crystalline Solids

journal homepage: www.elsevier.com/locate/jnoncrysol

A new idea of modeling shear band in metallic glass based on the concept of distributed dislocation

Xiaotao Li [a,*], Ruitao Qu [b], Wei Rao [c], Xiaoyu Jiang [d]

[a] Institute for Advanced Study, Chengdu University, Chengdu 610106, PR China
[b] State Key Laboratory of Solidification Processing, Northwestern Polytechnical University, Xi'an 710072, PR China
[c] State Key Laboratory of Nonlinear Mechanics, Institute of Mechanics, Chinese Academy of Sciences, Beijing 100190, PR China
[d] School of Mechanics and Engineering, Southwest Jiaotong University, Chengdu 610031, PR China

ARTICLE INFO

Keywords:
Shear band
Metallic glasses
Distributed dislocation
Void
Notch
Finite element

ABSTRACT

Shear bands are closely linked with the plasticity and fracture behaviors of metallic glasses (MGs). This work proposes a new idea to predict shear bands by continuously distributed dislocations. The dislocations are unreal and used to model the plastic deformation of shear band. The possible positions of shear band initiation are determined based on the elastic stress field, and the direction and length of shear band propagation are determined by the distributed dislocation technique. Finite element simulations based on constitutive model are carried out to compare with the theoretical modeling. Two examples are considered, i.e., shear bands near a void and a notch under tensile loading. The results show that the theoretically predicted shear band morphology is well consistent with the finite element simulations, which verifies the validation of using distributed dislocations to predict shear bands. This work provides a new way to model shear band, and it has potential applications in predicting shear band morphology and fracture behaviors in MGs.

1. Introduction

Metallic glasses (MGs) have attracted much attention due to their superior strength and high elastic strain. However, MGs are lack of ductility and often caused abrupt quasi-brittle failure at room temperature. In order to improve their ductility, shear bands, as the main plastic carrier of MGs, have been a research hotspot. Usually, shear bands initiate at the stress concentrators [1,2], and then propagate along the specific planes [2]. When a shear band propagates throughout the specimen, the strength of the MG is weakened quickly and an abrupt fracture will follow shortly. In fact, the formation of shear bands is regarded as a prelude of fracture of MGs.

Seeing that reasonable prediction of shear banding is of significance to analyze the failure behaviors of MGs, the research on shear banding has been received extensive interest in recent years. To deeply reveal the mechanisms of shear band initiation and propagation, numerous experimental observations [1,3–10], theoretical methods [2,11,12], molecular dynamics simulations [13–16] and finite element (FE) simulations [17–22] have been conducted. From the perspective of experimental observation, Demetriou et al. [3] observed the evolution of shear banding near a notch and fracture behaviors in Pb-based MG. Gludovatz et al. [4] observed size-dependence modes of shear banding near a notch and crack growth in Pb-based MG. Qu et al. [1] found the propagation modes of shear bands in Pb-based and Ti-based MGs under compression. From the perspective of theoretical analysis, Packard and Schuh [2] analyzed shear-banding path and yield stress of MGs under Hertzian pressure. In the analyses, maximum shear stress criterion, pressure-modified maximum shear stress criterion and shear plane criterion were applied, respectively. The shear plane criterion was verified to be more accurate than others, which demonstrates the shear band propagation is attributed to the stresses along the specific shear plane, rather than the maximum stress. The above investigations have revealed many interesting phenomena. However, how to capture the spatio-temporal evolution nature of shear bands is still a challenge. Therefore, Yang et al. [13] carried out atomistic simulations to study the evolution of shear bands and crack nucleation in Zr-based MG under nanoindentation; Wang et al. [15] studied the influence of nanoscale pores on shear banding, strength and ductility of Zr-based MG by molecular dynamics simulations.

However, atomistic simulations can only be applied to calculate nanoscale models, and the statistical phenomena and collective behaviors associated with multiple shear band interactions under typical

* Corresponding author.
E-mail address: lixiaotao@cdu.edu.cn (X. Li).

https://doi.org/10.1016/j.jnoncrysol.2021.121328
Received 11 August 2021; Received in revised form 24 November 2021; Accepted 27 November 2021
Available online 20 December 2021

experimental conditions cannot be captured. Instead, FE simulation based on constitutive models of MG is a feasible solution. Anand and Su [17] proposed a Mohr-Coulomb type constitutive model and the model was implemented in FE simulations to simulate shear bands in MGs. Based on the proposed constitutive model, Su and Anand [18] simulated the evolution of shear bands under indentation; Tandaiya et al. simulated shear band morphology near mode I crack tip [19] and mixed-mode crack tip [20]. These simulated results based on the constitutive model match well with experimental observations, which illustrates the availability of the constitutive model to simulate shear bands. Hence, FE simulations based on the constitutive model will be applied to verify our new idea of predicting shear band.

In this paper, we adopt a new way to predict the propagation of shear band. The idea is to replace the shear deformation along a shear band by continuously distributed dislocations, and the length and direction of shear band propagation are determined based on the distributed dislocation technique (DDT). In principle, the distributed dislocation can be applied to model complex deformation modes of various materials, and it has been successfully applied to model cracks [23–26], boundaries [23,27], plasticity [28–30] and dislocation slip [31–34], while no research work has been found it was used to model shear band. In fact, shear banding is a relative movement of two parts of MG along a specific shear plane, and the shear deformation can be modeled by continuously distributed glide dislocations according to the DDT. The integral equation of dislocation density can be established based on the condition that the stresses along shear bands satisfy the corresponding yield conditions (such as Mohr-Coulomb criterion [35] or the ellipse criterion [36]). The dislocation density function is obtained by solving the integral equation, and then the direction and length of shear band can be determined. This work will provide a new way to study shear banding in MGs and broaden the application scope of the DDT.

This paper is organized as follows. In Section 2, the solution scheme is presented. In order to compare with the proposed theoretical method, the FE simulations based on the constitutive model developed by Anand and Su are conducted. The constitutive modeling is introduced in this section. The theoretical solution of shear banding near a void and a notch is presented based on the DDT. In Section 3, the results are shown and discussed. The comparison of shear band morphology between theoretical modeling and FE simulation is shown. Finally, Section 4 is the concluding remark.

2. Solution scheme

2.1. Constitutive modeling

2.1.1. Main equations for shear-band-deformation respond in MGs

The constitutive model used in this work was proposed by Anand and Su [17], which was based on the hypothesis of finite deformation and Mohr-Coulomb yield condition. It has been verified that the constitutive model is valid to model shear band in Zr-based MGs under various loading modes, such as tension, compression, indentation, etc. In the constitutive model, it is assumed that plastic flow occurs by shearing accompanied by dilatation relative to some slip systems, and there are six potential slip systems:

$$\left.\begin{array}{ll}\mathbf{s}^{(1)}=\mathbf{e}_1\cos\widehat{\theta}+\mathbf{e}_3\sin\widehat{\theta}, & \mathbf{m}^{(1)}=\mathbf{e}_1\sin\widehat{\theta}-\mathbf{e}_3\cos\widehat{\theta};\\ \mathbf{s}^{(2)}=\mathbf{e}_1\cos\widehat{\theta}-\mathbf{e}_3\sin\widehat{\theta}, & \mathbf{m}^{(2)}=\mathbf{e}_1\sin\widehat{\theta}+\mathbf{e}_3\cos\widehat{\theta};\\ \mathbf{s}^{(3)}=\mathbf{e}_1\cos\widehat{\theta}+\mathbf{e}_2\sin\widehat{\theta}, & \mathbf{m}^{(3)}=\mathbf{e}_1\sin\widehat{\theta}-\mathbf{e}_2\cos\widehat{\theta};\\ \mathbf{s}^{(4)}=\mathbf{e}_1\cos\widehat{\theta}-\mathbf{e}_2\sin\widehat{\theta}, & \mathbf{m}^{(4)}=\mathbf{e}_1\sin\widehat{\theta}+\mathbf{e}_2\cos\widehat{\theta};\\ \mathbf{s}^{(5)}=\mathbf{e}_2\cos\widehat{\theta}+\mathbf{e}_3\sin\widehat{\theta}, & \mathbf{m}^{(5)}=\mathbf{e}_2\sin\widehat{\theta}-\mathbf{e}_3\cos\widehat{\theta};\\ \mathbf{s}^{(6)}=\mathbf{e}_2\cos\widehat{\theta}-\mathbf{e}_3\sin\widehat{\theta}, & \mathbf{m}^{(6)}=\mathbf{e}_2\sin\widehat{\theta}+\mathbf{e}_3\cos\widehat{\theta};\end{array}\right\} \tag{1}$$

where $\mathbf{s}^{(k)}$ is a slip direction and $\mathbf{m}^{(k)}$ is a normal direction of slip plane, and their superscript denotes the slip system. $\{\mathbf{e}_i,\ i=1,2,3\}$ are the orthonormal principal directions of stress tensor, and the stress tensor is symmetric and it has the spectral representation $\boldsymbol{\sigma}=\sigma_i\mathbf{e}_i\otimes\mathbf{e}_i$ (σ_i is the principal stress and $\sigma_1\geq\sigma_2\geq\sigma_3$). $\widehat{\theta}=\frac{\pi}{4}+\frac{\arctan\mu}{2}$, where μ is the internal friction coefficient. The resolved shear and compressive normal stresses on each slip system can be given by

$$\tau^{(k)}=\mathbf{s}^{(k)}\cdot\boldsymbol{\sigma}\mathbf{m}^{(k)},\ \ \sigma^{(k)}=\mathbf{m}^{(k)}\cdot\boldsymbol{\sigma}\mathbf{m}^{(k)}. \tag{2}$$

Hence, Mohr-Coulomb yield criterion for each slip system can be written as $\tau^{(k)}-\mu\sigma^{(k)}\geq c$, where c is the cohesion. Shear band will be nucleated and propagated when the Mohr-Coulomb yield condition is achieved in any one slip system. Once the shear band is generated, the cohesion in the shear band will be decreased and the strain softening will appear. The cohesion function is defined as

$$c=\tau_0+b\left(1-\frac{\eta}{\eta_0}\right)^q, \tag{3}$$

where τ_0 is the initial cohesion. b, q and η_0 are material parameters. η is the plastic volumetric strain, and it can be determined by its rate function

$$\dot{\eta}=g_0\left(1-\frac{\eta}{\eta_0}\right)^p\sum_{k=1}^{6}v^{(k)},\ \ \eta(0)=0, \tag{4}$$

where $v^{(k)}$ is the shearing rate, and it is defined as

$$v^{(k)}=v_0\left(\frac{\tau^{(k)}}{c+\mu\sigma^{(k)}}\right)^{1/m}, \tag{5}$$

where v_0 and m are material parameters. Further, the plastic stretching tensor is given by

$$\mathbf{D}^p=\sum_{k=1}^{6}v^{(k)}\left[\mathrm{sym}\left(\mathbf{s}^{(k)}\otimes\mathbf{m}^{(k)}\right)+g_0\left(1-\frac{\eta}{\eta_0}\right)^p\mathbf{m}^{(k)}\otimes\mathbf{m}^{(k)}\right]. \tag{6}$$

To measure the plastic shear deformation of shear band, an equivalent plastic shear strain (EPSS) is defined as

$$\mathrm{EPSS}=\int_0^t|\mathrm{D}_0^p|\mathrm{d}t, \tag{7}$$

where $\mathbf{D}_0^p$ is the deviatoric tensor of $\mathbf{D}^p$.

2.1.2. FE implementation and verification of constitutive model

In this work, the constitutive model is implemented in the FE software ABAQUS by writing a user material subroutine VUMAT [37], and the MG with composition $Zr_{56.06}Cu_{23.39}Ni_{15.54}Ta_{2.27}Al_{1.62}Ti_{1.11}$ is considered. The related material parameters used in the FE simulations are listed in Table 1, which are obtained from the previous studies [17,18,20,38–40]. The Young's modulus and Poisson's ratio are 89 GPa [18] and 0.36 [39], respectively. The internal friction coefficient is taken as 0.04 [40]. The strain rate sensitivity parameter is usually taken from 0.005 to 0.02 [17,18,20,38], and it is taken as 0.01 in this work. The

Table 1.
Material parameters in the present FE simulation [17,18,20,38–40].

Material parameters	Value	Material parameters	Value
Young's modulus, E	89 GPa	Cohesion function exponent, q	2
Poisson's ratio, ν	0.36	Dilatancy function exponent, p	0.5
Dilatancy function coefficient in tension, g_0	0.4	Internal friction coefficient, μ	0.04
Dilatancy function coefficient in compression, g_0	0.04	Initial cohesion, τ_0	820 MPa
Reference shear strain rate, v_0	0.001 s^{-1}	Cohesion function coefficient, b	80 MPa
Strain rate sensitivity parameter, m	0.01	Saturation free volume, η_0	0.005

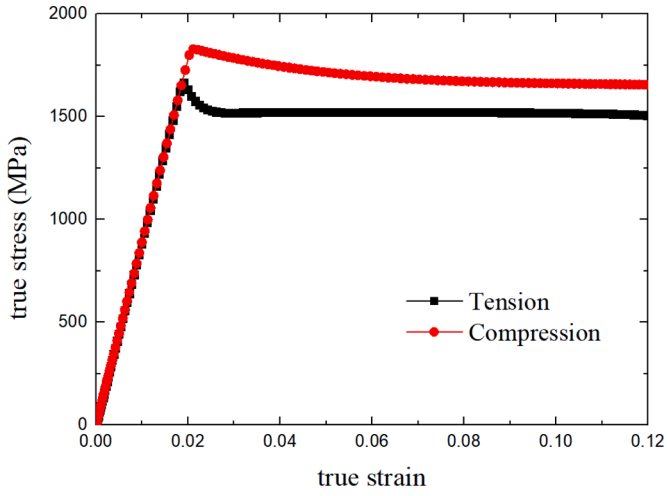

Fig. 1.. Stress–strain response of a single C3D8R element under tension or compression.

parameters in the dilatancy function and the cohesion function are obtained from the Ref. [18].

To verify the validity of the VUMAT programing, a single-element model under uniaxial tension and compression loading was calculated. The true stress-strain response is plotted in Fig. 1. The results show that the compressive yield stress is higher than the tensile yield stress and the strain softening in tension is much faster than it in compression, which is consistent with the experiment results [41]. It should be noted that the damage behaviors in shear band do not be considered, and the strain softening is only considered, as shown in Fig. 1. Previous works [18,20] have verified that this way is feasible to simulate shear bands in Zr-based MGs. To further verify the validity of the VUMAT programing, a two-dimensional plane strain FE model is established, as shown in Fig. 2 (a). The plate contains a circle micro-void in its center under uniform tension and compression. The element type is CPE4R. The contour of EPSS under tension and compression is plotted in Fig. 2(b) and (c), respectively. Generally, the formation of shear bands is regarded as a prelude of fracture of MGs, and the propagation of shear bands causes the final fracture. In Fig. 2, shear bands are initiated from a micro-scale void and propagated through the entire specimen. The inclined angles of shear band are 50° and 44° in tension and compression, respectively. In fact, the difference of mechanical behaviors between tension and compression is an important characteristic in MGs, such as fracture angle and fracture stress [36,41]. The present simulations are consistent with the mechanical characteristics of MGs, and thus the VUMAT programing is feasible to simulate shear band.

2.2. *Distributed dislocation modeling of shear band*

According to the DDT, a dislocation with infinitesimal Burgers vector can serve as a kind of strain nuclei in solids, and various deformation modes can be modeled by distributed dislocations as long as the density of distributed dislocations is reasonable. The opening-mode deformation (mode I), the shearing-mode deformation (mode II), and the tearing-mode deformation (mode III) of the crack can be modeled by the continuous glide dislocations, the climb dislocations, and the screw dislocations, respectively. Hence, a mixed-mode crack can be replaced by mixed-mode dislocations. Fig. 3(a)–(c) show the modeling of a mixed-mode crack by continuously distributed dislocations. The dislocation is denoted by the red symbol '⊥'. Similarly, a shear band (blue line) could be also modeled by continuously distributed dislocations, as shown in Fig. 3(d)–(f). In fact, the main difference between modeling shear band and modeling crack is the boundary condition along the dislocation strips. For the crack problem, the crack plane is traction-free. For MGs, a shear band will be generated if the critical condition $\tau + \mu\sigma = \tau_0$ is reached (for simplicity, assuming a Mohr-Coulomb yield criterion, although the ellipse criterion has been found to be better for MGs [36,

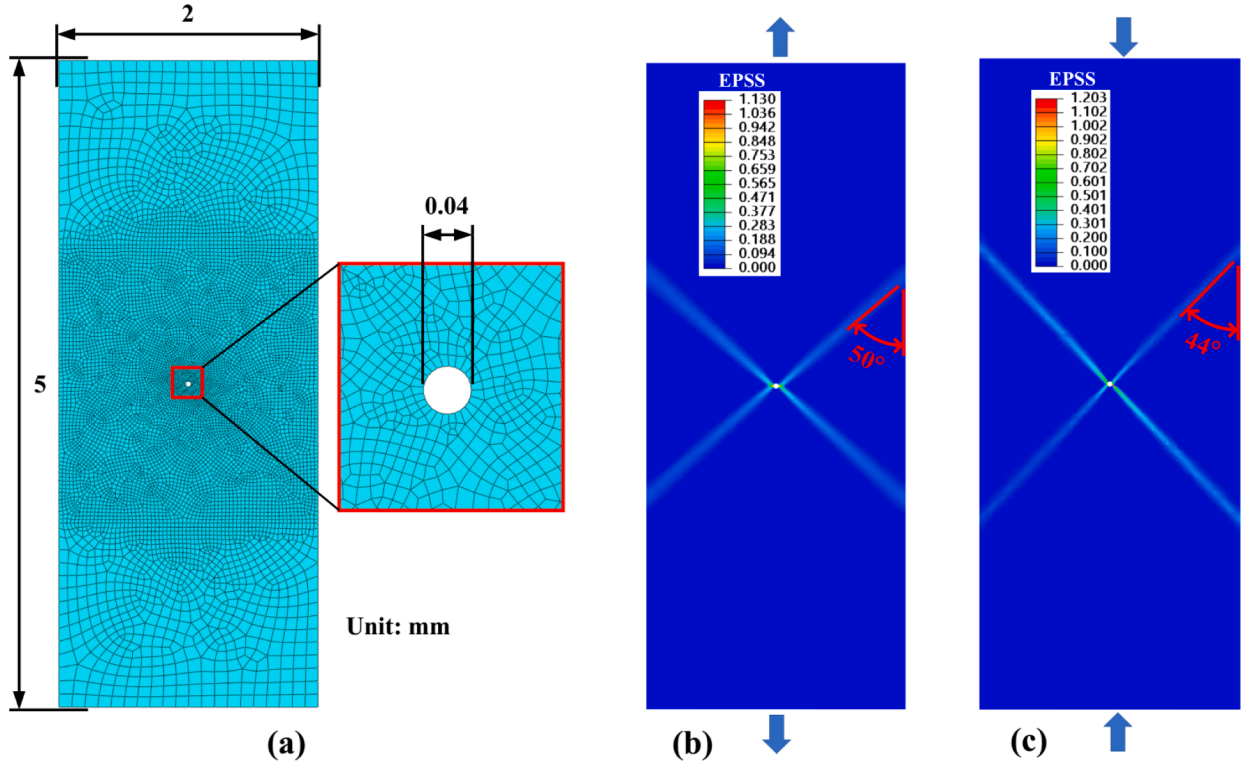

Fig. 2.. Simulation of fracture angle in plane strain under uniform tension and compression: (a) FE model, a two-dimensional plate containing a micro-void; (b) contour of EPSS under tension; (c) contour of EPSS under compression.

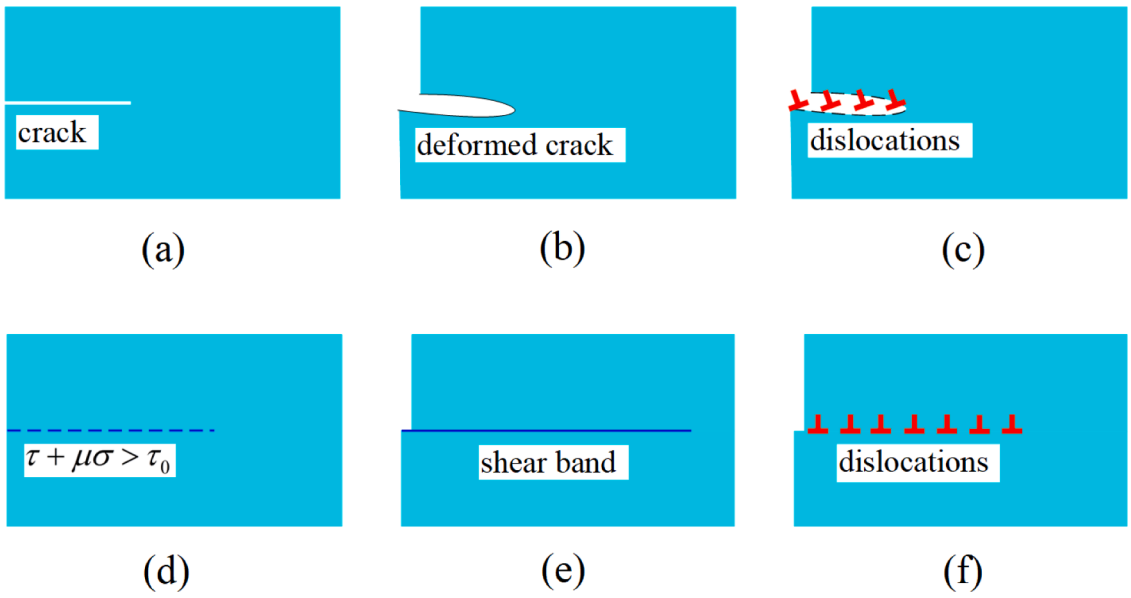

Fig. 3.. Schematic of using continuously distributed dislocations to model cracking and shear banding: (a) and (b) the crack will slide and open under external loading; (c) sliding and opening-mode deformation of the crack plane are replaced by continuously dislocations distributed along the crack; (d) the stress components along a specific plane in MGs satisfy $\tau+\mu\sigma>\tau_0$, and then a shear band will be initiated and propagated (e); (f) the shear deformation of shear band is modeled by continuously dislocations distributed along the shear band.

42]). Here, τ and σ are the elastic shear and normal stresses along the shear plane; μ is the internal friction coefficient; τ_0 is the cohesion. Shear banding is an in-plane shearing-mode deformation, and thus, theoretically, it can be modeled by the glide dislocations distributed along the shear plane. In the shear band, the yield condition $\tau + \mu\sigma = \tau_0$ must be satisfied. Although the concept of dislocation has been used for interpreting the shear plastic deformation of MGs some decades ago [43], it is now generally accepted that the plastic deformation of MGs relies on nanoscale structural defects like shear transformation zone [44], rather than dislocations. Thus, it should be pointed out that the distributed dislocations in the present theoretical modeling are unreal, and they are used only to model the shearing deformation of shear bands.

Next, two examples will be considered, and our idea will be verified from the simple to the complex. The first is shear banding near a square void under uniform tension. Due to the stress concentration at the corners of the void, shear band will be initiated from the corners. The stresses are concentrated at the corner, namely, it is a point-type stress concentrator (two-dimensional plane is considered). Thus, the shear band morphology is relatively simple. The second example is a more complex case, that is shear banding near a notch. This is a line-type stress concentrator. Thus, the shear band morphology is more complex.

2.3. Shear banding near a square void

In this section, the problem of shear banding near a square void is considered. The FE model for this problem is firstly introduced, and then the theoretical solution based on the DDT is presented.

2.3.1. The FE model

The FE model is a two-dimensional square plate containing a square void in the center of the model under plane strain state, and it is established by ABAQUS/Explicit. The model is subjected to the uniaxial uniform tensile load in the vertical direction. The length of the model is 24 mm and the length of the void is 2 mm. The length of the model exceeds ten times of the void length, so the free surface has little effect on the plastic deformation near the void. The element type is CPE4R.

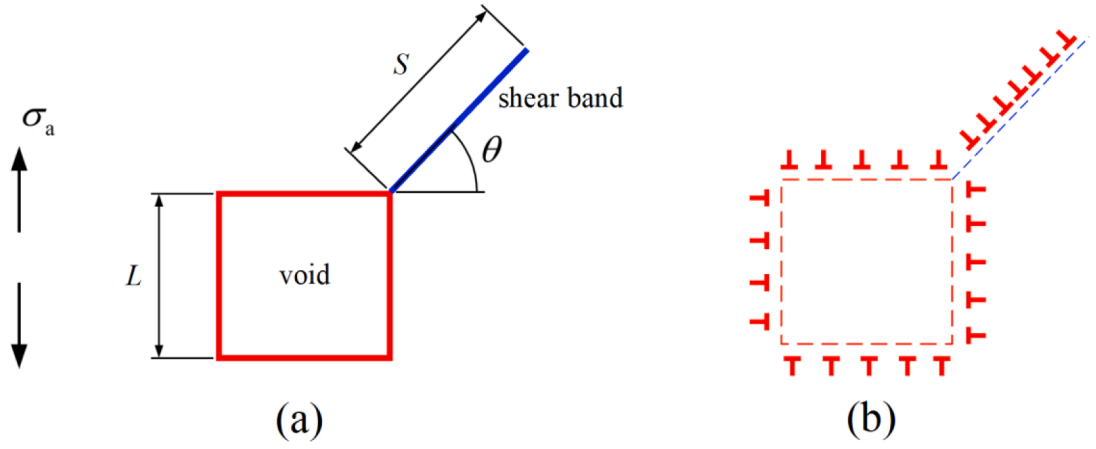

Fig. 4.. Schematic of theoretical modeling of shear banding near the square void: (a) an infinite plane contains a square void under uniaxial uniform tensile load σ_a, and a shear band is generated due to the stress concentration at the corner of the void; (b) the void is cut out from an infinite plane by a kinked crack, and then the kinked crack and the shear band are modeled by continuously distributed dislocations. $L = 2$ mm, S is unknow and need to be solved.

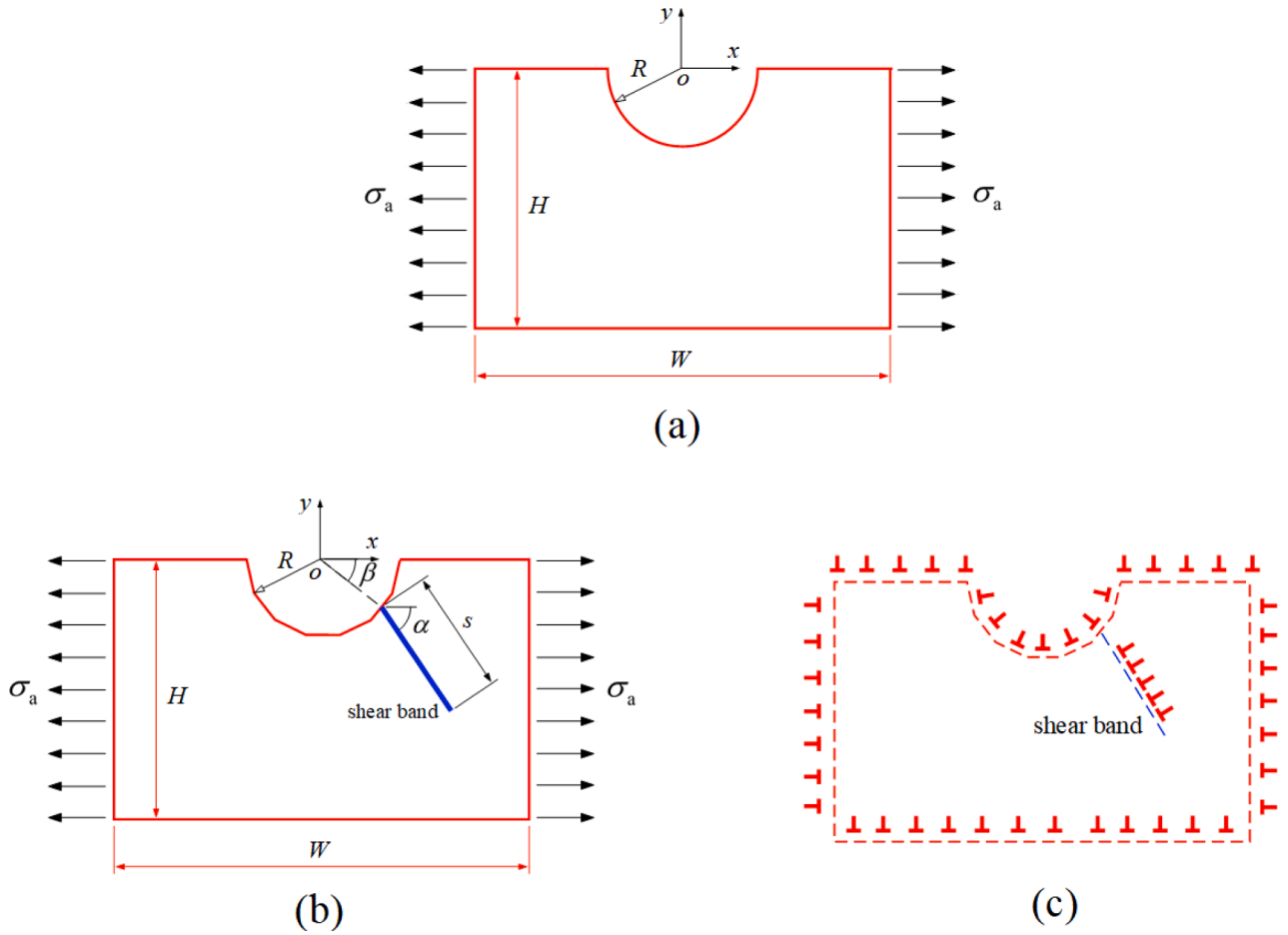

Fig. 5.. Schematic of the model of a rectangular specimen containing a notch: (a) FE model, a rectangular specimen containing a half of circle notch under uniaxial tensile load; (b) theoretical model, a two-dimension rectangular specimen containing a half of polygonal notch and an arbitrary shear band originating from the notch; (c) the specimen of the theoretical model is cut out from an infinite plane by a kinked crack, and then the kinked crack and the shear band are replaced by continuously distributed dislocations. $R = 1.5$ mm, $H = 10$ mm and $W = 16$ mm.

There are 35,742 elements in the model. The length of the elements near the void is 0.04 mm. The biggest element is in the boundary of the plate and the length is 2 mm.

2.3.2. *Theoretical solution based on the DDT*

In this section, we use distributed dislocations to model shear band near a void. The stress field induced by dislocations in an infinite plane can be obtained easily. For simplicity, an infinite plate containing a square void and a shear band under uniaxial tensile load is considered in the theoretical model. Due to the void, an image force on the dislocations will be generated, and the stress field is complicated in this case. For simplicity, the problem of an infinite plane containing a void is considered as the equivalent problem of an infinite plane containing a kinked crack. The kinked crack is located along the boundaries of the void, namely, the void is cut out by the kinked crack(. According to the DDT, the crack can be modelled as an array of dislocations, so the present problem is simplified as an infinite plane containing dislocations.

As shown in Fig. 4(a), in the theoretical model, an infinite plate contains a square void. Although an infinite plate is considered in the theoretical model and a finite plate is simulated in the FE model, there is little difference between them. This is because the free surface has little effect on the deformation near the void when the distance between the void and the free surface surpasses ten times the size of the void [45]. As shown in Fig. 4, a shear band (blue line) is generated due to the stress concentration at the corner. S is the length of the shear band and θ is the inclined angle. The positive value of θ is defined as the anticlockwise direction. In order to compare with the FE simulation, L is fixed at 2 mm.

According to the analysis in Section 2.2, the kinked crack and shear banding can be modeled by continuously distributed dislocations, as shown in Fig. 4(b). The problem is described as an infinite elastic plane containing five dislocation strips (four dislocation strips are distributed along the boundaries of the void and one dislocation strip is along the shear band) under uniaxial uniform tensile load. The stress field in the global coordinate induced by multiple dislocation strips in an infinite elastic plane has been derived, as shown in Appendix. Hence, the stress components due to five dislocation strips can be given by

$$\overline{\sigma}_{ij}^{\text{total}}(x,y) = \sum_{n=1}^{5} \overline{\sigma}_{ij}\left(x,y,\theta_n,\alpha_n,d_n,l_n,B_{xn},B_{yn}\right) ij = xx\, xy \text{ or } yy, \tag{8}$$

where d_n is the distance between the origin of the global coordinate and the center of the dislocation strip "n"; l_n is the half length of the dislocation strip; θ_n is the orientation angle and α_n is the inclined angle (see Appendix); B_{xn} and B_{yn} are the components of dislocation density function, which are unknown. Because the shear band is modeled by glide dislocations, the component B_{yn} of the shear band is equal to zero. The stress field of the problem shown in Fig. 4 can be obtained by the superposition of the stresses induced by dislocations and the applied stresses, so it can be given by

$$\sigma_{ij}(x,y) = \overline{\sigma}_{ij}^{\text{total}}(x,y) + \widetilde{\sigma}_{ij}(x,y)\, ij = xx\, xy \text{ or } yy, \tag{9}$$

Here, $\widetilde{\sigma}_{ij}(x,y)$ is induced by the applied tensile load, and $\widetilde{\sigma}_{xx} = \widetilde{\sigma}_{xy} = 0$, $\widetilde{\sigma}_{yy} = \sigma_a$. In order to obtain the dislocation density function, related equations need to be established by stress boundary conditions. The

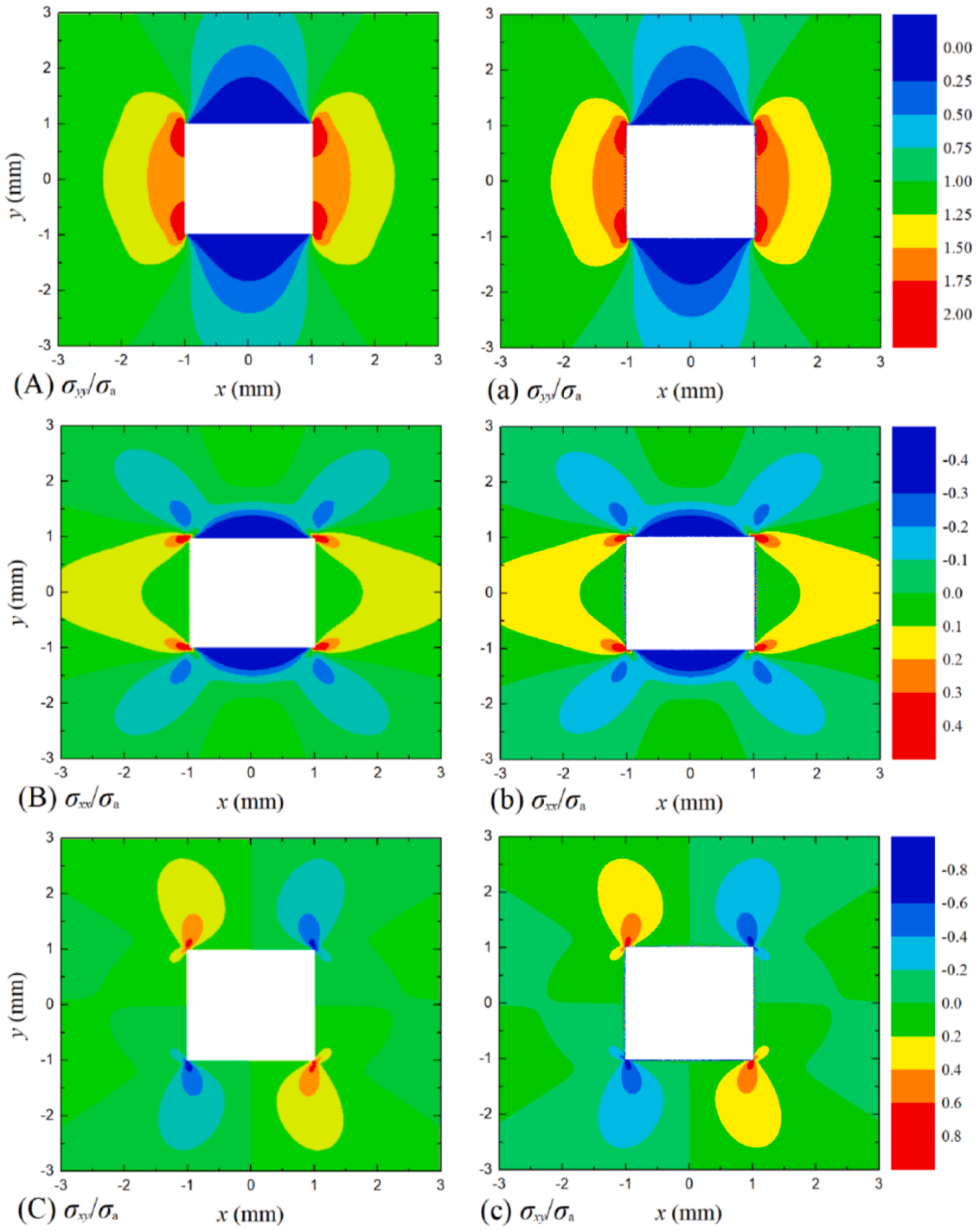

Fig. 6.. Comparison of normalized elastic stress field near the void between theoretical modeling (right) and FE simulation (left).

boundary conditions are described that the kinked crack plane is traction-free and the shear band satisfies $\tau+\mu\sigma = \tau_0$. The stress components along each dislocation strip can be calculated by the relationship between the local coordinate and the global coordinate (Eq. (10)) and the Mohr stress transformation (Eq. (11)).

$$x = d_n\cos\theta_n + x_n\cos\alpha_n - y_n\sin\alpha_n, \tag{10a}$$

$$y = d_n\sin\theta_n + x_n\sin\alpha_n + y_n\cos\alpha_n. \tag{10b}$$

$$\sigma_{y_n y_n} = \sigma_{xx}(x,y)(\sin\alpha_n)^2 + \sigma_{yy}(x,y)(\cos\alpha_n)^2 - \sigma_{xy}(x,y)\sin 2\alpha_n, \tag{11a}$$

$$\sigma_{x_n y_n} = -\{\sigma_{xx}(x,y) - \sigma_{yy}(x,y)\}(\sin\alpha_n\cos\alpha_n) + \sigma_{xy}(x,y)\cos 2\alpha_n. \tag{11b}$$

Hence, the integral equations of dislocation density functions can be established by the stress boundary conditions of the void and the shear band, as shown in Eq. (12).

$$\sigma_{y_n y_n} = \sigma_{x_n y_n} = 0 \text{ for the void boundaries}, \tag{12a}$$

$$\sigma_{x_n y_n} + \mu\sigma_{y_n y_n} = \tau_0 \text{ for the shear band}. \tag{12b}$$

In Eq. (12), the unknowns are B_{xn}, B_{yn} and S. The analytical solution of the integral equations is difficult to obtain, but the numerical solution can be solved by the Gauss-Chebyshev quadrature method [23,46,47].

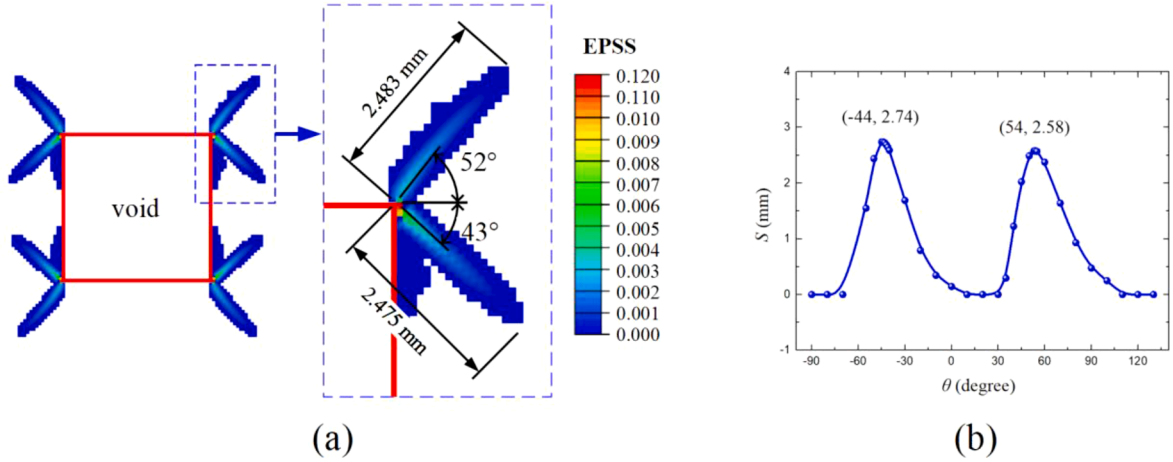

Fig. 7.. (a) contour chart of EPSS by FE simulation; (b) theoretical results of using dislocations to model shear banding: the variation of shear band length versus its possible direction. The tensile load is σ_a/τ_0=1.

The core idea of the numerical method is that the continuous integral equations can be discretized as a series of nonlinear equations. The numerical solution is relatively accurate as long as the discretized number is large enough. Giving a specific value of θ, the corresponding value of S can be obtained by Eq. (12). Therefore, the variation of S versus θ can be obtained. In this paper, a hypothesis is proposed that the shear band will propagate along the direction in which S reaches its maximal value. Based on the hypothesis, the propagating direction and length of shear band can be determined.

2.4. Shear banding near a notch

In this section, we consider the problem of shear banding near a notch in a finite-size plate. Firstly, the FE model is introduced in Section 2.4.1. Secondly, the theoretical solution is presented based on the DDT in Section 2.4.2.

2.4.1. The FE model

This is a two-dimensional rectangular plate containing a half-circle notch under plane strain state, and it is established by ABAQUS/Explicit. The schematic of the FE is shown in Fig. 5(a). The uniform tensile load is applied on the left and right boundaries. The geometric dimensions of this model are $R = 1.5$ mm, $H = 10$ mm and $W = 16$ mm. The element type is CPE4R. There are 58,776 elements in the model. The smallest element near the notch is 0.008 mm.

2.4.2. Theoretical solution based on the DDT

In this section, a finite plate containing a notch under uniform tensile load is considered. For simplicity, the problem of a finite plane containing a notch is considered as the equivalent problem of an infinite plane containing a kinked crack. The kinked crack is located along the boundaries of the finite plate, and the plate is cut out by the kinked crack from an infinite plane. According to the DDT, the crack can be modelled as an array of dislocations, so the present problem is simplified as an infinite plane containing dislocations. As shown in Fig. 5(b) and (c), a finite-size plate contains a notch under the uniform tensile load. For simplification, the circle notch is replaced by a regular polygon (14 sides). Due to the notch, the stress concentration is generated near the notch. Hence, we assume that shear banding is nucleated from the notch. Based on the DDT, the boundaries of the specimen and the shear band are modeled by continuously distributed dislocations along them. The present problem can be described that an infinite plane contains 13 dislocation strips (12 dislocation strips along the boundaries and 1 dislocation strip along the shear band) and the tensile load is applied on the left and right boundaries of the specimen. The problem of multiple dislocation strips in an infinite plane has been solved in Appendix, and the stress field can be given by

$$\sigma_{ij}(x,y) = \overline{\sigma}_{ij}^{\text{total}}(x,y) = \sum_{n=1}^{13} \overline{\sigma}_{ij}\left(x,y,\theta_n,\alpha_n,d_n,l_n,B_{xn},B_{yn}\right) ij = xx\, xy \text{ or } yy. \tag{13}$$

Notice that the stress field in Eq. (13) is only contributed by dislocations without the contribution of applied load, which is different from the problem of the void. In the problem of the void, the external load is remote uniform tension, while the tensile load is applied on the dislocation strips in the present problem.

The stress components along each dislocation strip can be calculated by Eqs. (10) and (11). The boundary conditions of the problem in Fig. (12) are that the uniform tensile loading is applied on the right and left dislocation strips and other dislocation strips along the boundaries are traction-free. According to these conditions, the integral equations can be established in Eq. (14).

$$\sigma_{y_n y_n} = \sigma_a \text{ fortheleftandrightboundaries}, \tag{14a}$$

$$\sigma_{x_n y_n} = 0 \text{ fortheleftandrightboundaries}, \tag{14b}$$

$$\sigma_{y_n y_n} = \sigma_{x_n y_n} = 0 \text{ forotherboundaries}, \tag{14c}$$

$$\sigma_{x_n y_n} + \mu\sigma_{y_n y_n} = \tau_0 \text{ fortheshearband}. \tag{14d}$$

Eq. (14) can be solved by the Gauss-Chebyshev quadrature method, and the shear band length s can be obtained. The variation of s versus β and α can be calculated. β and α are two parameters to determine the orientation and the inclined angle of the shear band. In order to examine the range of shear band propagation, β is taken every 10°. In doing so, the maximal value of s can be obtained, and then the length and inclined angle of shear band propagation can be determined.

3. Results and discussions

In Section 3, the results are shown and discussed. Firstly, the theoretical elastic stress field is verified by FE simulations. Secondly, the shear band morphology predicted by the DDT is compared with FE simulations. The void problem is analyzed in Section 3.1 and the notch problem is discussed in Section 3.2.

3.1. Shear banding near a void

Because shear bands in MGs are usually initiated at stress concentrators, we must first examine the exactitude of the elastic stress field by the DDT to determine the stress concentration zones. The comparison of

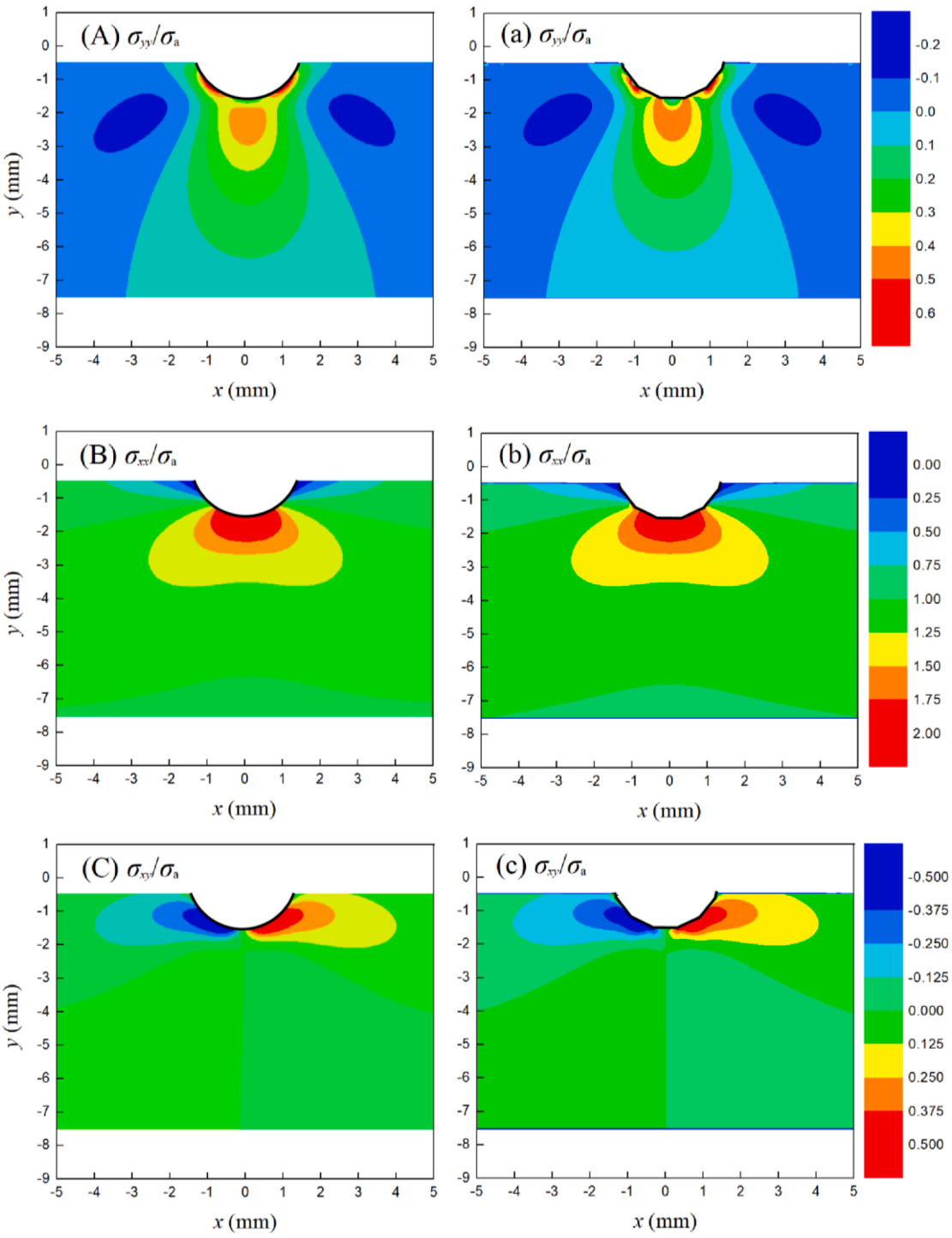

Fig. 8.. Comparison of elastic stress field near the notch between theoretical modeling (right) and FE simulation (left).

normalized elastic stress field between FE simulations and theoretical calculations by the DDT is shown in Fig. 6. The results show little difference between theoretical modeling and FE simulation, which is a mutual validation between them. The stress concentration zones are located at the vicinity of the corners of the void. Hence, shear bands are expected to be initiated from the corners. The shear band propagating length can be obtained by the DDT. The contour chart of equivalent plastic shear strain (EPSS) by FE simulations was plotted in Fig. 7(a), and the variation of S versus θ was plotted in Fig. 7(b).

The results in Fig. 7 show the propagating length and direction of shear bands. In the FE simulation, the propagating length S is 0.993 mm at θ=52° and S = 0.99 mm at θ=−43° In the theoretical modeling, S is 1.032 mm at θ=54° and S = 1.096 mm at θ=−44° The relative errors of propagating length between FE simulation and theoretical modeling are 3.8% and 9.7%. The relative errors of propagating direction are 3.8% and 2.3%. The relative error of shear band propagating direction is within 5% and it is within 10% for the shear band propagating length. The results illustrate it is reasonable that the shear band will propagate along the direction in which S reaches its maximal value, and more importantly, the DDT is valid to predict shear bands in MGs.

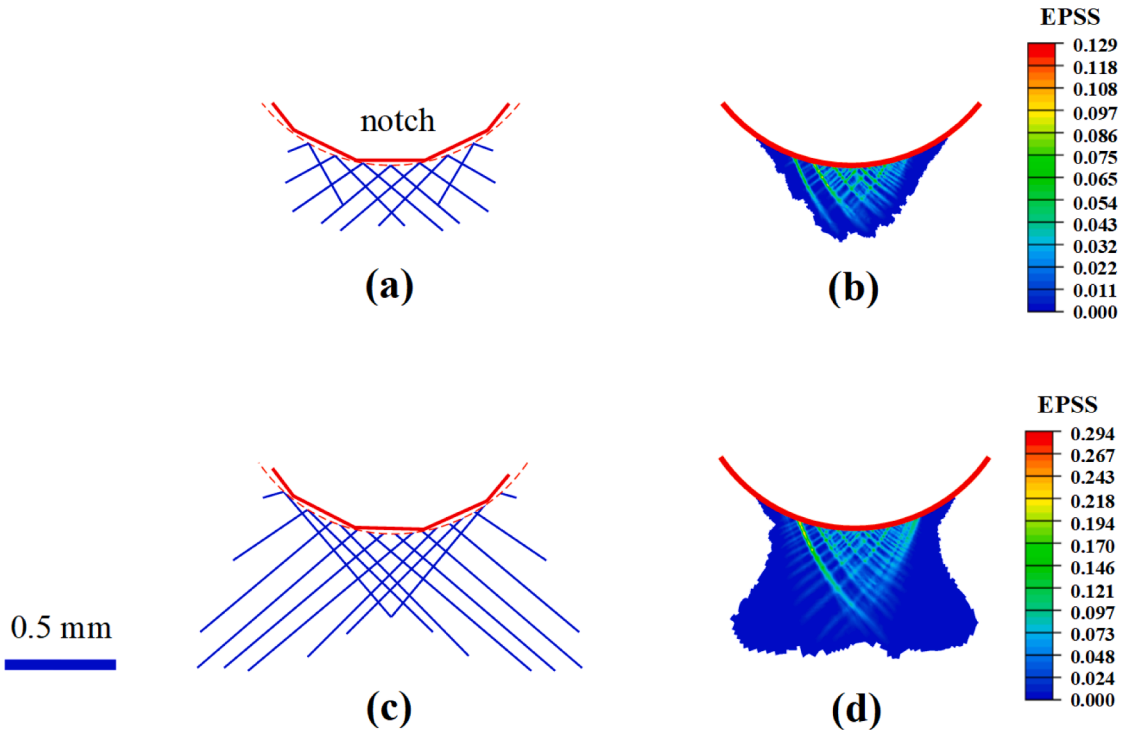

Fig. 9.. Comparison of shear band morphology between theoretical prediction and FE simulation: shear bands (blue lines) predicted by theoretical modeling at σ_a/τ_0=1 (a) and at σ_a/τ_0=1.25 (c); Contour chart of EPSS simulated by FE method at σ_a/τ_0=1 (b) and at σ_a/τ_0=1.25 (d).

3.2. Shear banding near a notch

In this section, the problem of shear bands near a notch in MGs is analyzed. The comparison of normalized elastic stress field near the notch between theoretical modeling (labelled by lowercase letters) and FE simulation (labelled by uppercase letters) is shown in Fig. 8. The results show there is a little difference between them near the notch. There are two main reasons for the difference: 1) In the numerical solution, continuous dislocation density functions are discretized, which causes inaccurate stress distribution near dislocation strips; 2) In the theoretical modeling, a polygonal notch is used, which is an approximate model compared with the FE model. However, the difference is relatively small. In this paper, we focus on the prediction of shear band morphology, i.e., plastic zone shape and size. Compared with entire plastic zone, the difference of elastic stress field in the vicinity of the notch is insignificant. In the theoretical modeling, the shear band propagating direction and length are determined by the stresses along the shear band. Hence, as long as the stress field is relatively accurate, the simplification in the theoretical modeling is reasonable.

As shown in Fig. 9, the plastic zone under different tensile loads is determined by theoretical modeling and FE simulation. The results show the theoretical shear band morphology is relatively consistent with FE results. At σ_a/τ_0=1, shear bands are initiated and propagated along inclined planes, and the plastic deformation is generated under the notch. Under the notch, the normal stress is concentrated (as shown in Fig. 8), which causes a relatively large shear stress along the inclined planes. Thus, the Mohr-Coulomb yield condition is preferentially reached in the inclined plane under the notch. With increasing applied tension loading (at σ_a/τ_0=1.25), shear bands in the both sides of the notch propagate rapidly and become longer than shear bands under the notch. This is because the shear stress concentration zones are distributed in the both sides of the notch. With increasing tensile loading, plastic deformation near the notch is gradually dominated by shear banding in the both sides. In the previous experimental observations [3,5,48], there is a similar phenomenon, and the results show the shear bands in the both sides of the notch are predominant and eventually fractured along a shear band in one side. As a whole, the theoretical modeling of shear banding is relatively close to corresponding FE simulations, and the DDT is an effective tool to predict shear bands in MGs.

The previous experiments have shown that the propagating path of shear banding is curved in many cases [3–5,18], and shear bands propagate progressively under complex loading or uniaxial loading

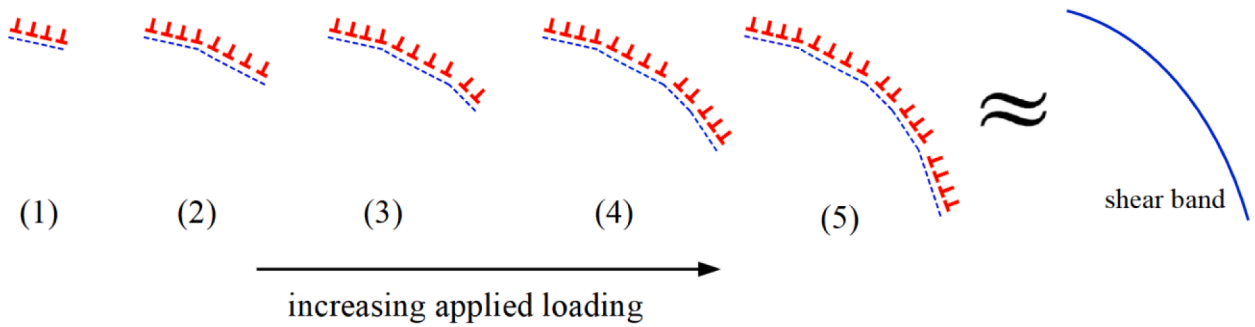

Fig. 10.. Schematic of the DDT to model a curved and progressive-propagating shear band.

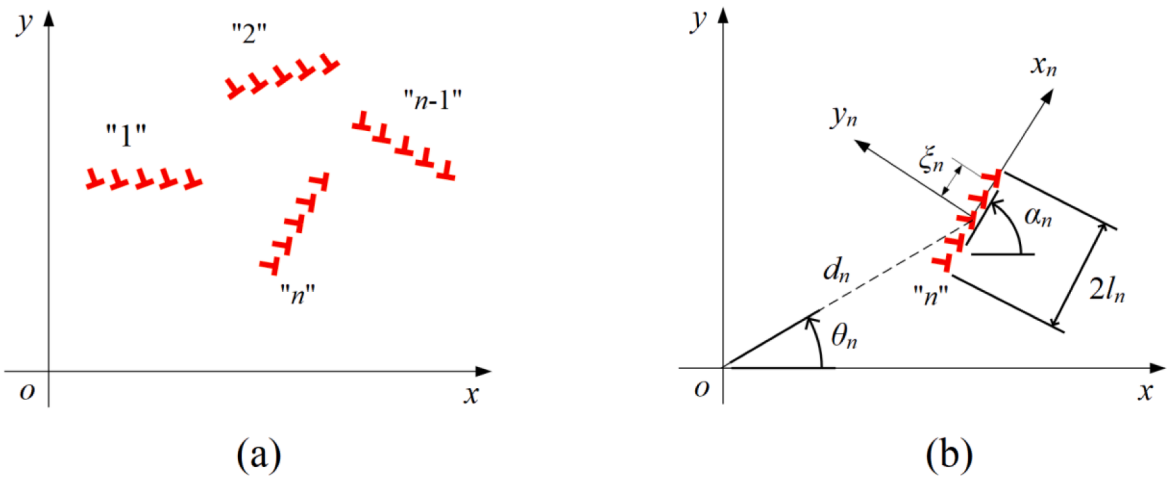

Fig. A1.. (a) an infinite elastic plane containing multiple arbitrarily located dislocation strips; (b) an infinite elastic plane containing an arbitrarily located dislocation strip.

before macroscopic yielding [1]. In the present theoretical modeling, shear band propagation is assumed as a straight line. In fact, a curve shear band can also be modeled by the DDT. With the increasing applied loading, the direction and length of shear band propagation can be determined step by step, as shown in Fig. 10. Certainly, the predicted shear band path is an approximation of the actual shear band. However, the predict path will be close to the actual path with the increasing calculation step. In future works, the DDT will be developed further to model more complex shear bands in MGs.

4. Concluding remarks

In this paper, the specimen boundaries and shear banding are modeled by continuously distributed dislocations. In doing so, the specimen with a complex-shaped geometry can be simplified as an infinite plane containing dislocations, which avoids to derive the image force on dislocations. Thus, the elastic stress field near a void and a notch is obtained easily, and then the stress concentration zones can be determined. According to the existing experimental observations [1,2], shear bands are initiated at the stress concentrators. The possible positions of shear banding initiation are determined by the stress concentration zones. We can distribute dislocations along these possible positions. According to stress boundary conditions, integral equations of dislocation density function can be established. The integral equations have a unique and self-consistent solution, so the length of shear band propagation can be obtained. For different possible directions of shear band, the different lengths can be obtained. Assuming the shear band will propagate along the direction in which the length reaches its maximal value, the direction and length of shear band can be determined uniquely.

In order to examine the validation of the theoretical modeling, FE simulations are carried out based on the constitutive model proposed by Anand and Su [17]. For the problem of shear banding near a void, the predicted and simulated length and direction of shear bands are very close. The relative error of shear band propagating direction is within 5% and it is within 10% for the shear band propagating length. For the problem of shear banding near a notch under tension loading, the predicted and simulated shear band morphology is quite similar, and the variation tendency of plastic zone with the increasing tensile load is also the same. The results preliminarily demonstrate that the DDT is valid to predict shear bands in MGs. Besides, FE simulation requires a very dense mesh to simulate shear band morphology, which leads to a large amount of computation. In the present way, the dislocation density function need only to solve, and the length and direction of shear band can be obtained easily. In summary, this work provides a new idea to model shear bands and it has fundamental and potential applied values in predicting shear band morphology and fracture behaviors of MGs.

Data availability

The raw/processed data required to reproduce these findings will be made available on request.

CRediT authorship contribution statement

Xiaotao Li: Conceptualization, Methodology, Investigation, Writing – original draft, Writing – review & editing. **Ruitao Qu:** Methodology, Investigation, Writing – review & editing. **Wei Rao:** Software, Validation, Writing – review & editing. **Xiaoyu Jiang:** Investigation, Writing – review & editing.

Declaration of Competing Interest

The authors declare that they have no known competing financial interests or personal relationships that could have appeared to influence the work reported in this paper.

Acknowledgments

This work was financially supported by the National Natural Science Foundation of China (Grant No. 51771205 and 11472230).

Appendix: Solution of an infinite elastic plane containing multiple dislocation strips

The solution of an infinite elastic plane containing multiple dislocation strips will be presented based on the DDT. Firstly, an arbitrarily located dislocation strip is considered. As shown in Fig. A1(b), a local coordinate is established; d_n is the distance between the origins of global and local coordinates; l_n is the half length of the dislocation strip; θ_n is the orientation and α_n is the inclined angle. The positive value of θ_n and α_n is defined as the anticlockwise direction.

The stress components in the local coordinate induced by an edge dislocation located at the position (ξ_n, 0) with the Burgers vectors b_{xn} and b_{yn} can be given by

$$\overline{\sigma}_{ij} = \frac{2m}{\pi(\kappa+1)}\left\{b_{xn}G_{xij}(x_n, y_n, \xi_n) + b_{yn}G_{yij}(x_n, y_n, \xi_n)\right\}\ ij = x_nx_n, x_ny_n \text{ or } y_ny_n. \tag{A1}$$

Here, m is shear modulus; κ is Kolosov's constant, κ=(3-ν)/(1+ν) for plane stress and κ=(3-ν) for plane strain (ν is Poisson's ratio). G_{xij} and G_{yij} are the dislocation influence functions, and their expressions can be obtained by

$$\begin{Bmatrix} G_{xx_nx_n} \\ G_{xx_ny_n} \\ G_{xy_ny_n} \end{Bmatrix} = \begin{Bmatrix} -\frac{y_n}{r^4}\left[3(x_n-\xi_n)^2 + y_n^2\right] \\ \frac{x_n-\xi_n}{r^4}\left[(x_n-\xi_n)^2 - y_n^2\right] \\ \frac{y_n}{r^4}\left[(x_n-\xi_n)^2 - y_n^2\right] \end{Bmatrix}, \begin{Bmatrix} G_{yx_nx_n} \\ G_{yx_ny_n} \\ G_{yy_ny_n} \end{Bmatrix} = \begin{Bmatrix} \frac{x_n-\xi_n}{r^4}\left[(x_n-\xi_n)^2 - y_n^2\right] \\ \frac{y_n}{r^4}\left[(x_n-\xi_n)^2 - y_n^2\right] \\ \frac{x_n-\xi_n}{r^4}\left[(x_n-\xi_n)^2 + 3y_n^2\right] \end{Bmatrix}; \tag{A2}$$

$$r^2 = (x_n-\xi_n)^2 + y_n^2. \tag{A3}$$

The stress components due to an array of continuously distributed dislocations can be obtained by integrating over the zone of the dislocation strip.

$$\overline{\sigma}_{ij} = \frac{2m}{\pi(\kappa+1)}\int_{-l_n}^{l_n}\left[B_{xn}(\xi_n)G_{xij}(x_n, y_n, \xi_n) + B_{yn}(\xi_n)G_{yij}(x_n, y_n, \xi_n)\right]d\xi_n\ ij = x_nx_n, x_ny_n \text{ or } y_ny_n. \tag{A4}$$

Here, B_{xn} and B_{yn} are the components of dislocation density function. The local coordinate system and the global coordinate system can be related by Eqs. (A5) and (A6).

$$x_n = -d_n\cos(\alpha_n - \theta_n) + x\cos\alpha_n + y\sin\alpha_n, \tag{A5}$$

$$y_n = d_n\sin(\alpha_n - \theta_n) - x\sin\alpha_n + y\cos\alpha_n. \tag{A6}$$

The stress field in the global coordinate can be obtained by the Mohr stress transformation

$$\begin{Bmatrix} \overline{\sigma}_{xx} \\ \overline{\sigma}_{yy} \\ \overline{\sigma}_{xy} \end{Bmatrix} = \begin{Bmatrix} \cos^2\alpha_n & \sin^2\alpha_n & -\sin2\alpha_n \\ \sin^2\alpha_n & \cos^2\alpha_n & \sin2\alpha_n \\ \sin\alpha_n\cos\alpha_n & -\sin\alpha_n\cos\alpha_n & \cos2\alpha_n \end{Bmatrix} \begin{Bmatrix} \overline{\sigma}_{x_nx_n} \\ \overline{\sigma}_{y_ny_n} \\ \overline{\sigma}_{x_ny_n} \end{Bmatrix}. \tag{A7}$$

The stress components induced by a dislocation strip have been obtained, and then the stress field due to multiple dislocation strips can be calculated by the superposition

$$\overline{\sigma}_{ij}^{\text{total}}(x, y) = \sum_{n=1}^{nd}\overline{\sigma}_{ij}\left(x, y, \theta_n, \alpha_n, d_n, l_n, B_{xn}, B_{yn}\right)\ ij = xxxy \text{ or } yy. \tag{A8}$$

Where, *nd* is the number of the dislocation strips.

References

[1] R. Qu, Z. Liu, G. Wang, Z. Zhang, Progressive shear band propagation in metallic glasses under compression, Acta Mater. 91 (2015) 19–33.
[2] C. Packard, C. Schuh, Initiation of shear bands near a stress concentration in metallic glass, Acta Mater. 55 (2007) 5348–5358.
[3] M.D. Demetriou, M.E. Launey, G. Garrett, J.P. Schramm, D.C. Hofmann, W. L. Johnson, et al., A damage-tolerant glass, Nat. Mater. 10 (2011) 123–128.
[4] B. Gludovatz, D. Granata, K.V. Thurston, J.F. Löffler, R.O. Ritchie, On the understanding of the effects of sample size on the variability in fracture toughness of bulk metallic glasses, Acta Mater. 126 (2017) 494–506.
[5] R. Narayan, D. Raut, U. Ramamurty, A quantitative connection between shear band mediated plasticity and fracture initiation toughness of metallic glasses, Acta Mater. 150 (2018) 69–77.
[6] D. Zhou, X. Zhao, B. Li, N. Hou, Z. Ma, T. Sun, et al., Shear-band-to-crack transition in bulk metallic glasses under quasi-static and dynamic shearing, J. Non Cryst. Solids 521 (2019), 119484.
[7] R. Qu, D. Tönnies, L. Tian, Z. Liu, Z. Zhang, C.A. Volkert, Size-dependent failure of the strongest bulk metallic glass, Acta Mater. 178 (2019) 249–262.
[8] S.-H. Joo, H. Kato, K. Gangwar, S. Lee, H.S. Kim, Shear banding behavior and fracture mechanisms of Zr55Al10Ni5Cu30 bulk metallic glass in uniaxial compression analyzed using a digital image correlation method, Intermetallics 32 (2013) 21–29.
[9] Y. Liu, C. Liu, A. Gali, A. Inoue, M. Chen, Evolution of shear bands and its correlation with mechanical response of a ductile Zr55Pd10Cu20Ni5Al10 bulk metallic glass, Intermetallics 18 (2010) 1455–1464.
[10] S. Jiang, S. Guo, Y. Huang, Z. Ning, P. Xue, W. Ru, et al., In situ study of the shear band features of a CuZr-based bulk metallic glass composite, Intermetallics 112 (2019), 106523.
[11] Y. Gao, L. Wang, H. Bei, T.-G. Nieh, On the shear-band direction in metallic glasses, Acta Mater. 59 (2011) 4159–4167.
[12] M. Jiang, W. Wang, L. Dai, Prediction of shear-band thickness in metallic glasses, Scr. Mater. 60 (2009) 1004–1007.
[13] Y. Yang, J. Luo, L. Huang, G. Hu, K.D. Vargheese, Y. Shi, et al., Crack initiation in metallic glasses under nanoindentation, Acta Mater. 115 (2016) 413–422.
[14] D. Şopu, Y. Ritter, H. Gleiter, K. Albe, Deformation behavior of bulk and nanostructured metallic glasses studied via molecular dynamics simulations, Phys. Rev. B 83 (2011), 100202.
[15] J. Wang, P.D. Hodgson, J. Zhang, W. Yan, C. Yang, Effects of pores on shear bands in metallic glasses: a molecular dynamics study, Comput. Mater. Sci. 50 (2010) 211–217.
[16] K. Albe, Y. Ritter, D. Şopu, Enhancing the plasticity of metallic glasses: shear band formation, nanocomposites and nanoglasses investigated by molecular dynamics simulations, Mech. Mater. 67 (2013) 94–103.
[17] L. Anand, C. Su, A theory for amorphous viscoplastic materials undergoing finite deformations, with application to metallic glasses, J. Mech. Phys. Solids 53 (2005) 1362–1396.
[18] C. Su, L. Anand, Plane strain indentation of a Zr-based metallic glass: experiments and numerical simulation, Acta Mater. 54 (2006) 179–189.
[19] P. Tandaiya, U. Ramamurty, G. Ravichandran, R. Narasimhan, Effect of Poisson's ratio on crack tip fields and fracture behavior of metallic glasses, Acta Mater. 56 (2008) 6077–6086.
[20] P. Tandaiya, U. Ramamurty, R. Narasimhan, Mixed mode (I and II) crack tip fields in bulk metallic glasses, J. Mech. Phys. Solids 57 (2009) 1880–1897.
[21] H. Ruan, L. Zhang, J. Lu, A new constitutive model for shear banding instability in metallic glass, Int. J. Solids Struct. 48 (2011) 3112–3127.
[22] W. Rao, J. Zhang, G. Kang, P.K. Liaw, Numerical simulation on the deformation behaviors of bulk metallic glass composites under uniaxial tension and compression, Compos. Struct. 187 (2018) 411–428.
[23] D.A. Hills, P. Kelly, D. Dai, A. Korsunsky, Solution of Crack Problems: the Distributed Dislocation Technique, Springer Science & Business Media, 2013.
[24] X. Li, X. Li, X. Jiang, Influence of a micro-crack on the finite macro-crack, Eng. Fract. Mech. 177 (2017) 95–103.
[25] X. Li, H. Yang, X. Zan, X. Li, X. Jiang, Effect of a micro-crack on the kinked macro-crack, Theor. Appl. Fract. Mech. 96 (2018) 468–475.
[26] K. Zhou, R. Wei, Modeling cracks and inclusions near surfaces under contact loading, Int. J. Mech. Sci. 83 (2014) 163–171.

[27] J. Zhang, Z. Qu, Q. Huang, L. Xie, C. Xiong, Interaction between cracks and a circular inclusion in a finite plate with the distributed dislocation method, Arch. Appl. Mech. 83 (2013) 861–873.
[28] X. Li, X. Li, H. Yang, X. Jiang, Analysis of the effect of a micro-crack on plastic zone of the edge macro-crack tip by macroscopic and microscopic methods, Eng. Fract. Mech. 201 (2018) 1–12.
[29] J. Codrington, A. Kotousov, Application of the distributed dislocation technique for calculating cyclic crack tip plasticity effects, Fatigue Fract. Eng. Mater. Struct. 30 (2007) 1182–1193.
[30] X. Li, M. Luo, W. Ma, Theoretical modeling of crack-tip plasticity by the distributed dislocation technique, Eng. Fract. Mech. 243 (2021), 107471.
[31] X. Li, J. Zhao, X. Zhang, X. Jiang, Revealing the inhibition mechanism of grain size gradient on crack growth in gradient nano-grained materials, Int. J. Solids Struct. 172 (2019) 1–9.
[32] X. Li, X. Jiang, Theoretical analyses of nanocrack nucleation near the main crack tip in nano and micro crystalline materials, Eng. Fract. Mech. 221 (2019), 106672.
[33] X. Li, S. Peng, X. Zhang, X. Jiang, Q. Wang, Microscopic and macroscopic analyses of the interaction mechanism between defect growth and dislocation emission in single-crystal aluminum, Fatigue Fract. Eng. Mater. Struct. 44 (2021) 3008–3022.
[34] X. Li, W. Ma, Molecular dynamics simulation and theoretical modeling of free surface effect on nanocrack initiation induced by grain boundary sliding in nanocrystalline materials, Mater. Lett. 304 (2021), 130647.
[35] P. Donovan, A yield criterion for Pd40Ni40P20 metallic glass, Acta Metall. 37 (1989) 445–456.
[36] R.T. Qu, Z.F. Zhang, A universal fracture criterion for high-strength materials, Sci. Rep. 3 (2013) 1117.
[37] ABAQUS. Theory Manuals, Version 6.5: Hibbitt, Karlsson and Sorensen; 2004.
[38] D. Raut, R.L. Narayan, Y. Yokoyama, P. Tandaiya, U. Ramamurty, Fracture of notched ductile bulk metallic glass bars subjected to tension-torsion: experiments and simulations, Acta Mater. 168 (2019) 309–320.
[39] J. Lu, G. Ravichandran, W.L. Johnson, Deformation behavior of the Zr41.2Ti13.8Cu12.5Ni10Be22.5 bulk metallic glass over a wide range of strain-rates and temperatures, Acta Mater. 51 (2003) 3429–3443.
[40] J.J. Lewandowski, P. Lowhaphandu, Effects of hydrostatic pressure on the flow and fracture of a bulk amorphous metal, Philos. Mag. A 82 (2002) 3427–3441.
[41] Z. Zhang, J. Eckert, L. Schultz, Difference in compressive and tensile fracture mechanisms of Zr59Cu20Al10Ni8Ti3 bulk metallic glass, Acta Mater. 51 (2003) 1167–1179.
[42] Z. Zhang, J. Eckert, Unified tensile fracture criterion, Phys. Rev. Lett. 94 (2005), 094301.
[43] J.J. Gilman, Mechanical behavior of metallic glasses, J. Appl. Phys. 46 (1975) 1625–1633.
[44] C.A. Schuh, T.C. Hufnagel, U. Ramamurty, Mechanical behavior of amorphous alloys, Acta Mater. 55 (2007) 4067–4109.
[45] M. Jafari, E. Ardalani, Stress concentration in finite metallic plates with regular holes, Int. J. Mech. Sci. 106 (2016) 220–230.
[46] F. Erdogan, G.D. Gupta, T. Cook, Numerical solution of singular integral equations. Methods of Analysis and Solutions of Crack Problems, Springer, Dordrecht, 1973, pp. 368–425.
[47] A.C. Kaya, F. Erdogan, On the solution of integral equations with strongly singular kernels, Q. Appl. Math. 45 (1987) 105–122.
[48] R. Qu, P. Zhang, Z. Zhang, Notch effect of materials: strengthening or weakening? J. Mater. Sci. Technol. 30 (2014) 599–608.